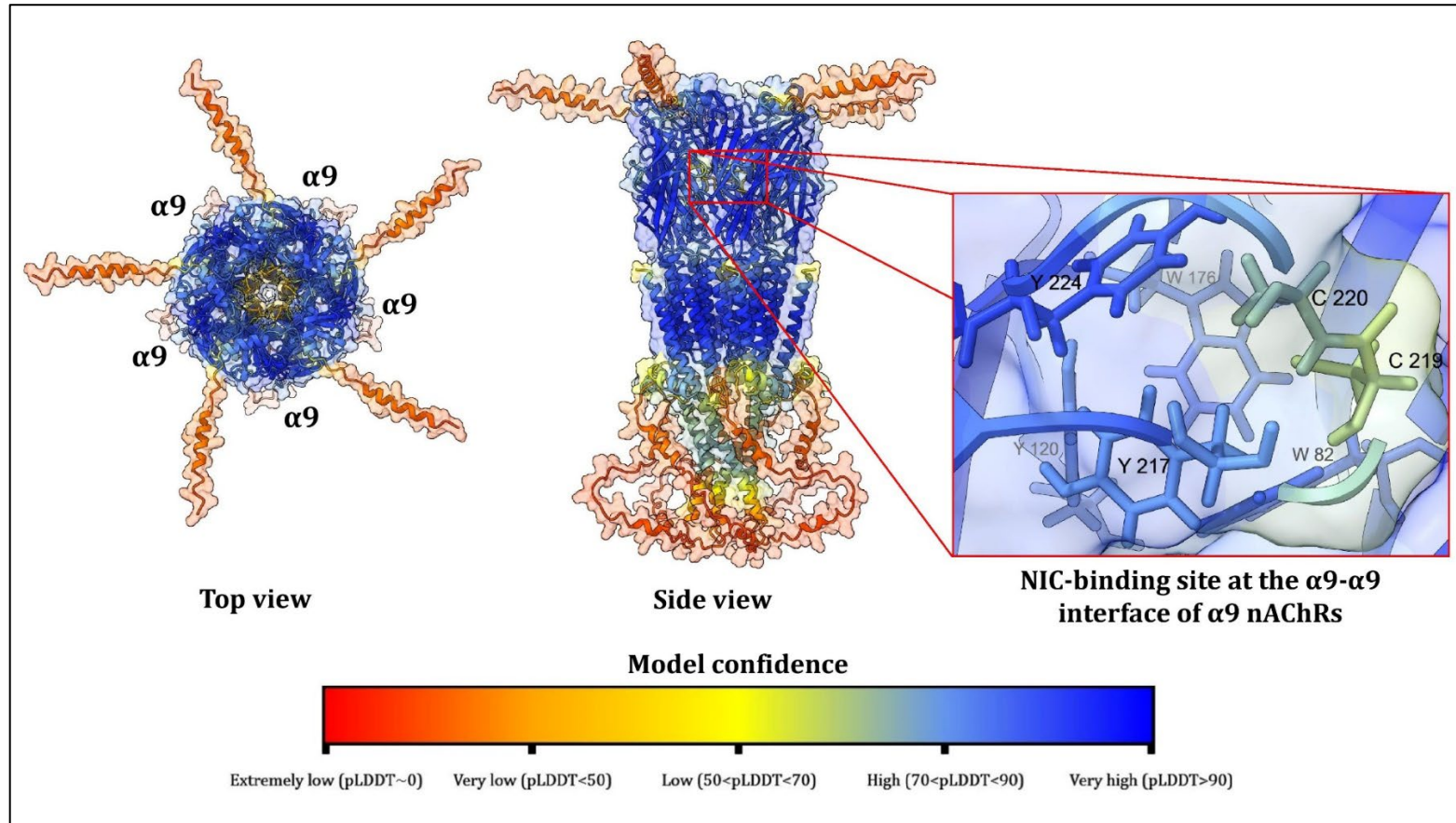
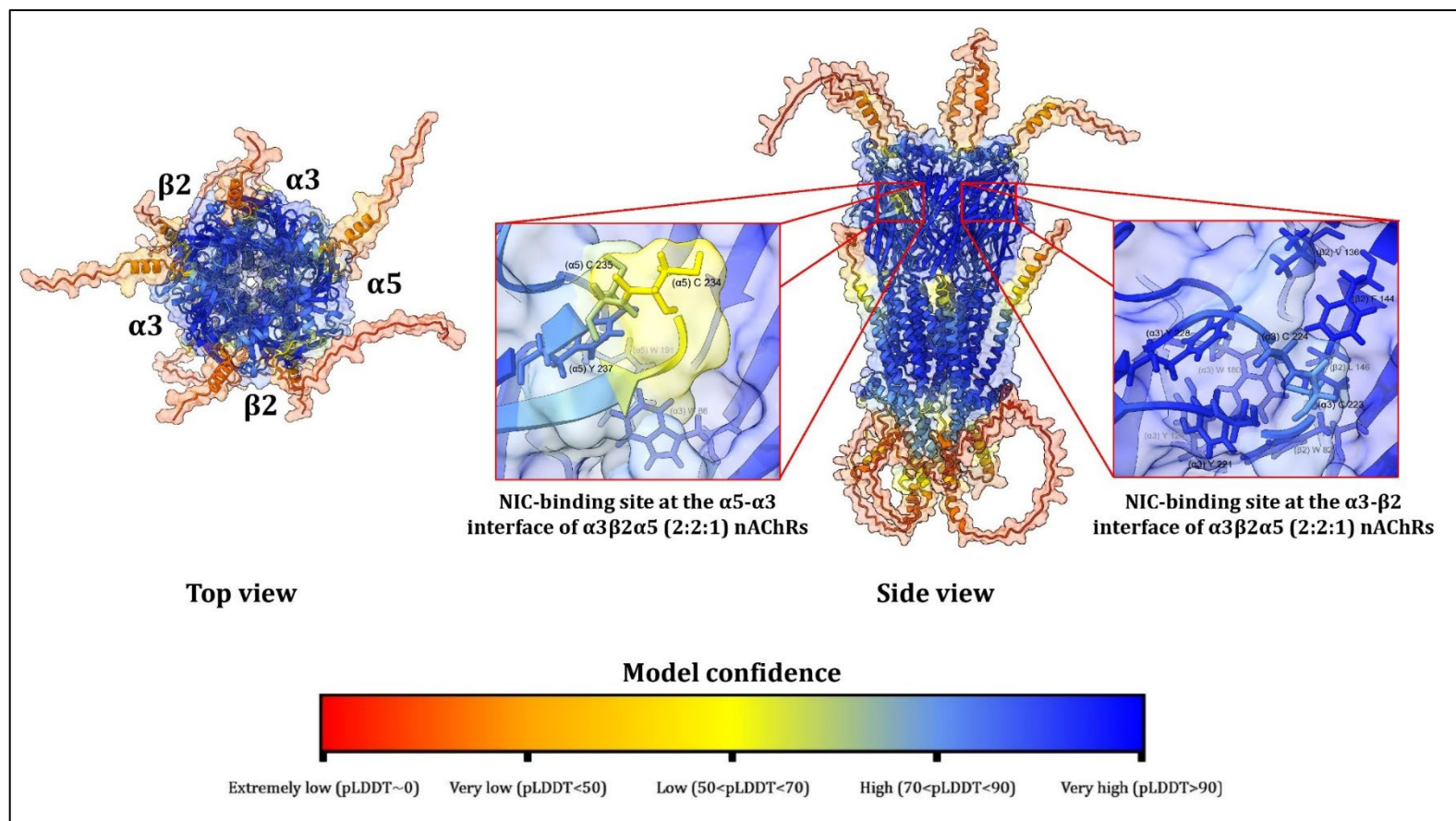


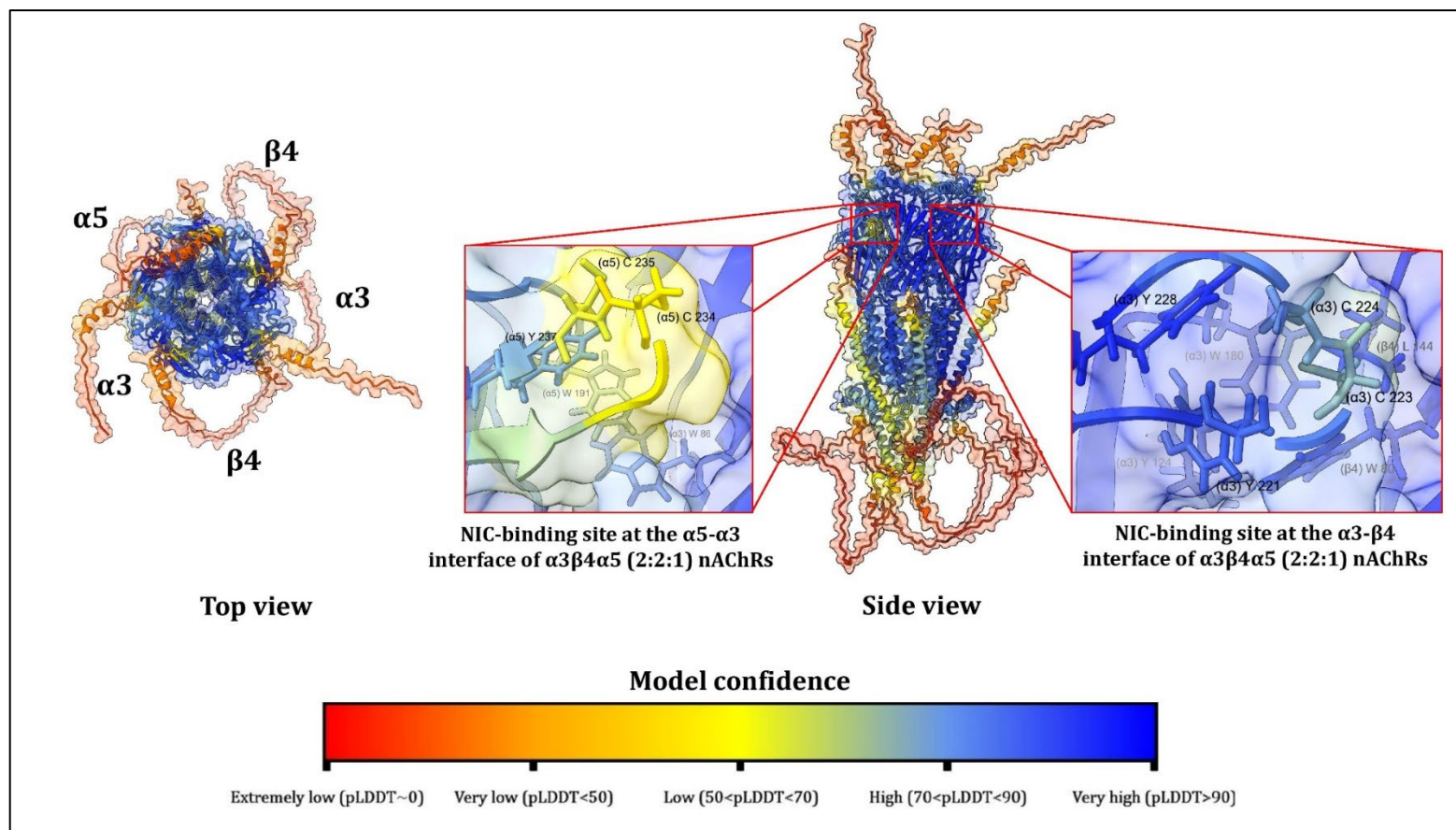
Supplementary material



Supplementary Figure S1. The AlphaFold multimer-modeled structure of homopentameric $\alpha 9$ nAChRs, the NIC-binding residues at the $\alpha 9$ - $\alpha 9$ interface and the confidence level expressed as pLDDT score.



Supplementary Figure S2. The AlphaFold multimer-modeled structure of heteropentameric $\alpha 3\beta 2\alpha 5$ (2:2:1 stoichiometry) nAChRs, the NIC-binding residues at the $\alpha 5$ - $\alpha 3$ and $\alpha 3$ - $\beta 2$ interfaces and the confidence level expressed as pLDDT score.



Supplementary Figure S3. The AlphaFold multimer-modeled structure of heteropentameric $\alpha 3\beta 4\alpha 5$ (2:2:1 stoichiometry) nAChRs, the NIC-binding residues at the $\alpha 5$ - $\alpha 3$ and $\alpha 3$ - $\beta 4$ interfaces and the confidence level expressed as pLDDT score.

Supplementary Table S1. The correspondence between the nicotine-binding residues of $\alpha 4$ subunit of $\alpha 4\beta 2$ nAChRs and $\alpha 9$, $\alpha 3$ and $\alpha 5$ subunits of $\alpha 9$, $\alpha 3\beta 2\alpha 5$ and $\alpha 3\beta 4\alpha 5$ subtypes of nAChRs

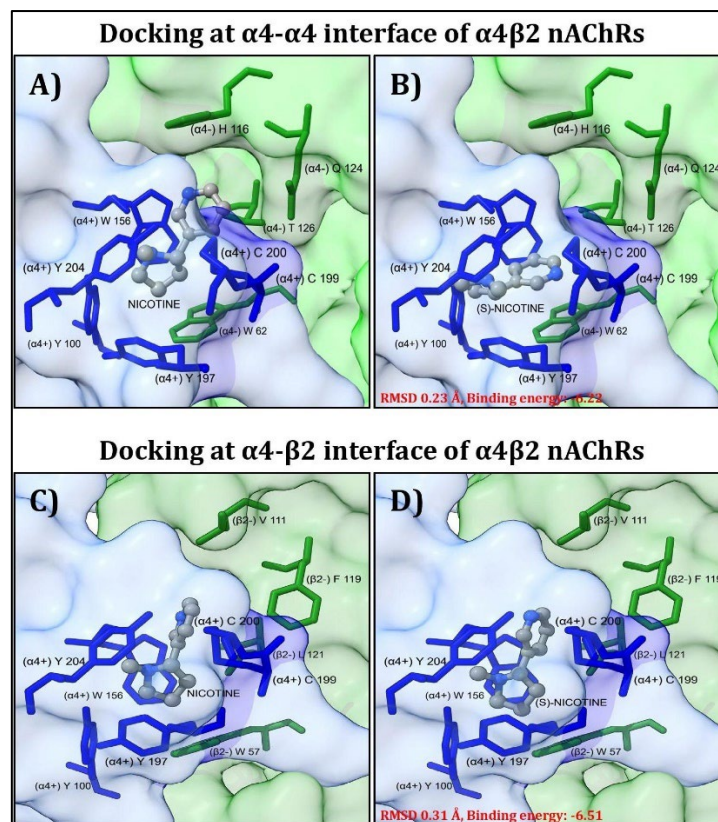
		NIC-binding site residues	Equivalent residues for NIC binding site in the predicted structures*				
		$\alpha 4\beta 2$ nAChRs (3 α :2 β , PDB ID 6CNK)	$\alpha 9$ nAChRs	$\alpha 3\beta 2\alpha 5$ (2:2:1) nAChRs		$\alpha 3\beta 4\alpha 5$ (2:2:1) nAChRs	
		$\alpha 4$ subunit	$\alpha 9$ subunit	$\alpha 3$ subunit	$\alpha 5$ subunit	$\alpha 3$ subunit	$\alpha 5$ subunit
α subunit	Principal side	Y100	Y120 (90.6)	Y124 (95.1)	-	Y124 (93.9)	-
		W156	W176 (92.6)	W180 (97)	W191 (92.2)	W180 (95.3)	W191 (82.3)
		Y197	Y217 (89.3)	Y221 (95.7)	-	Y221 (93.1)	-
		C199	C219 (79.6)	C223 (90)	C234 (66.5)	C223 (84.9)	C234 (63.8)
		C200	C220 (83.2)	C224 (92.8)	C235 (81.7)	C224 (88)	C235 (75.6)
		Y204	Y224 (95.3)	Y228 (97.9)	Y237 (93)	Y228 (97.2)	Y237 (89.4)
	Complementary side	W62	W82 (83.8)	W86 (96.3)	W98 (95.5)	W86 (95.9)	W98 (94.7)
		H116	-	-	-	-	-
		Q124	-	-	-	-	-
		T126	-	-	T161 (95.4)	-	T161 (94.9)

*The predicted Local Distance Difference Test (pLDDT) scores for the residues are indicated in brackets.

Supplementary Table S2. The correspondence between the nicotine-binding residues of $\alpha 4$ subunit of $\alpha 4\beta 2$ nAChRs and $\alpha 9$, $\alpha 3$ and $\alpha 5$ subunits of $\alpha 9$, $\alpha 3\beta 2\alpha 5$ and $\alpha 3\beta 4\alpha 5$ subtypes of nAChRs

β subunit		NIC-binding site residues	Equivalent residues for NIC-binding site in the predicted structures*	
		$\alpha 4\beta 2$ nAChRs (3 α :2 β , PDB ID 6CNK)	$\alpha 3\beta 2\alpha 5$ nAChRs (2:2:1)	$\alpha 3\beta 4\alpha 5$ nAChRs (2:2:1)
		$\beta 2$ subunit	$\beta 2$ subunit	$\beta 4$ subunit
	Principal side	Y95	Y120 (94.7)	Y118 (93.6)
		R149	R174 (96.7)	R172 (95.4)
		W151	W176 (93.5)	W174 (94)
		Y196	Y221 (95.7)	Y219 (93.8)
	Complementary side	W57	W82 (97.7)	W80 (96.7)
		V111	V136 (98)	-
		F119	F144 (98.2)	-
		L121	L146 (98)	L144 (96.8)

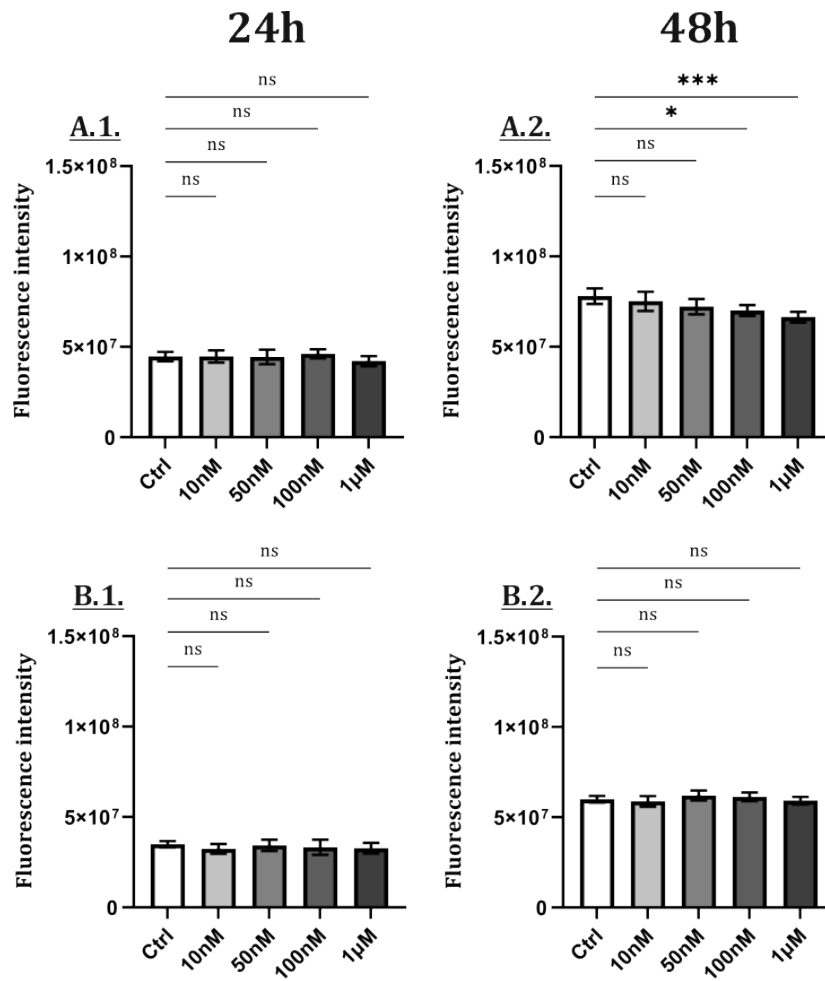
*The predicted Local Distance Difference Test (pLDDT) scores for the residues are indicated in brackets.



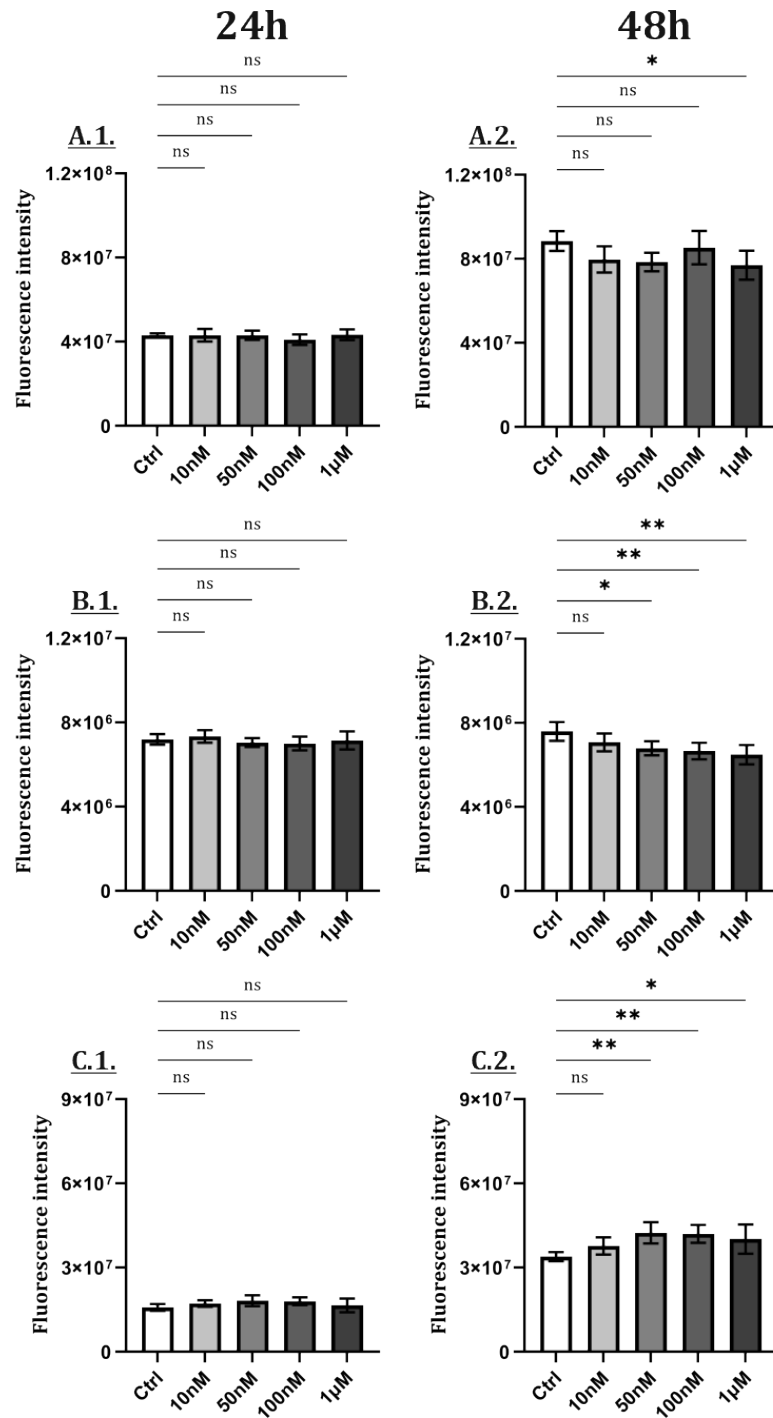
Supplementary Figure S4. The native position of NIC molecule (**A, C**) and the best theoretical binding pose of (S)-NIC (**B, D**) in the $\alpha 4$ - $\alpha 4$ interface (top panel) and $\alpha 4$ - $\beta 2$ interface (bottom panel) of $\alpha 4\beta 2$ nAChRs (3 α :2 β stoichiometry).

Supplementary Table S3. The binding energies, ligand efficiencies and the number of hydrogen (H) bonds formed for the best three binding positions of the ligands in the corresponding receptor

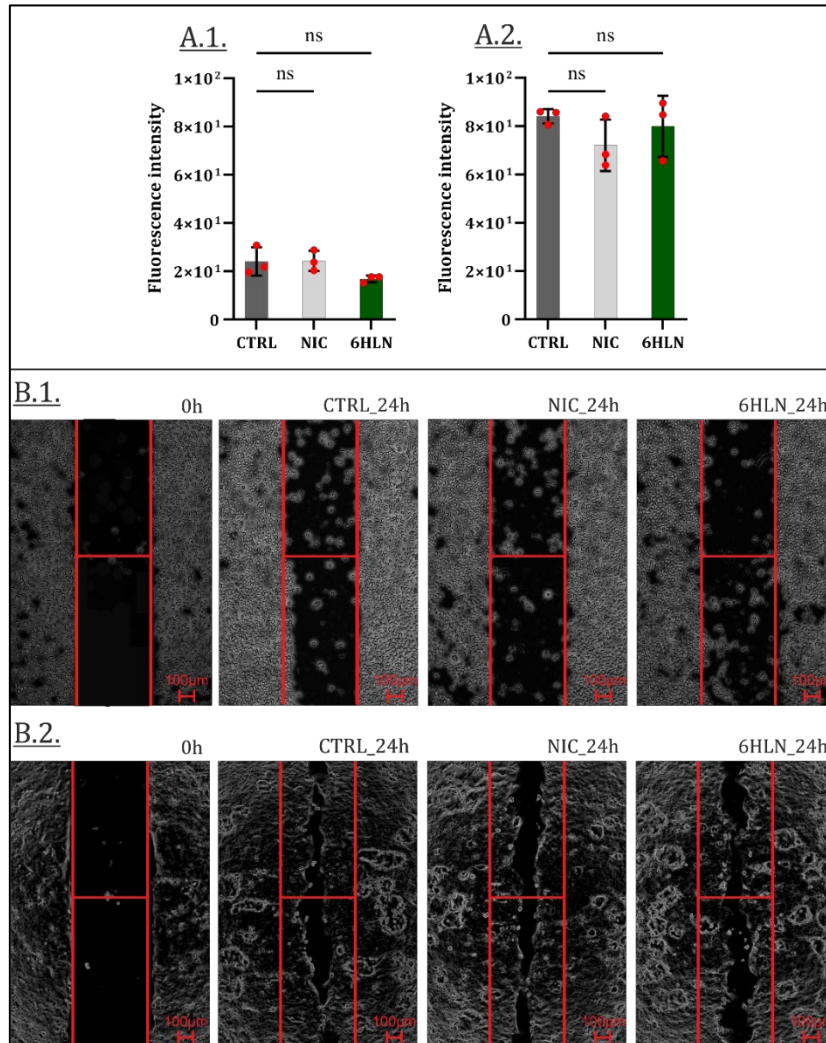
Receptor		Ligand	Binding energy	Ligand efficiency	H bonds formed
$\alpha 9$ nAChRs	$\alpha 9$ - $\alpha 9$ interface	(S)-Nicotine	-7.12	-0.59	0
			-6.07	-0.56	0
			-5.51	-0.46	0
		(S)-6-Hydroxynicotine	-7.38	-0.57	1
			-7.37	-0.57	1
			-7.28	-0.56	1
$\alpha 3\beta 2\alpha 5$ nAChRs (2:2:1 stoichiometry)	$\alpha 3$ - $\beta 2$ interface	(S)-Nicotine	-6.48	-0.54	0
			-6.48	-0.54	0
			-6.45	-0.54	0
		(S)-6-Hydroxynicotine	-6.69	-0.51	1
			-6.67	-0.51	1
			-6.52	-0.5	1
	$\alpha 5$ - $\alpha 3$ interface	(S)-Nicotine	-5.71	-0.48	0
			-5.71	-0.48	0
			-5.71	-0.48	0
		(S)-6-Hydroxynicotine	-6.28	-0.48	1
			-6.27	-0.48	1
			-6.24	-0.48	1
$\alpha 3\beta 4\alpha 5$ nAChRs (2:2:1 stoichiometry)	$\alpha 3$ - $\beta 4$ interface	(S)-Nicotine	-6.07	-0.51	0
			-6.06	-0.51	0
			-6.06	-0.51	0
		(S)-6-Hydroxynicotine	-6.55	-0.5	0
			-6.53	-0.5	0
			-6.52	-0.5	0
	$\alpha 5$ - $\alpha 3$ interface	(S)-Nicotine	-5.82	-0.49	1
			-5.78	-0.48	1
			-5.75	-0.48	1
		(S)-6-Hydroxynicotine	-6.05	-0.47	2
			-6.02	-0.46	2
			-6	-0.46	1



Supplementary Figure S5. Cellular viability 24 and 48 hours post incubation of 6HLN at different concentrations (10nM, 50nM, 100nM, and 1μM) in (A) 16HBE14o and (B) MCF10A normal cell lines. Values are means \pm S.D. (n = 5). ns - non-significant, * $p \leq 0.05$; *** $p \leq 0.001$.



Supplementary Figure S6. Cellular viability 24 and 48 hours post incubation of 6HLN at different concentrations (10nM, 50nM, 100nM, and 1μM) in (A) A549, (B) MCF-7, and (C) U87 cancer cell lines. Values are means \pm S.D. (n = 5). ns - non-significant, * $p \leq 0.05$; ** $p \leq 0.01$.



Supplementary Figure S7. Wound closure 24 hours post incubation of NIC / 6HLN (50nM) in 16HBE14o (A.1.) and MCF10A (A.2.) cells. B – Representative pictures: 16HBE14o (B.1.) and MCF10A (B.2.) cells. Values are means \pm S.D. (n = 3).